JOURNAL OF MATERIALS SCIENCE 33 (1998) 371–378

Undercooling in Co–Cu alloys and its effect on solidification structure

I. YAMAUCHI, N. UENO[‡], M. SHIMAOKA[§], I. OHNAKA
Department of Material Science and Processing, Faculty of Engineering of Osaka University 2-1, Yamada-oka, Suita, Osaka 565, Japan

Undercooling behaviour and solidification morphology change of various Co–Cu alloys were examined. Each alloy was melted in an alumina crucible under an argon atmosphere by high-frequency induction, and the cyclic heating and cooling was repeated several times in the temperature range between 1300 and 1850 K. The temperature change during the experiment was analysed under the Newtonian cooling assumption. The temperature curve showed that the undercooling in a first few cycles was negligibly small but it increased remarkably. The alloy was undercooled below the metastable liquid miscibility gap after the next several cycles. In these samples, liquid separation was observed. The homogeneously mixed spherical grains of copper-enriched phase were observed in cobalt-enriched matrix for the samples solidified immediately after the liquid separation. The two melts became coarser after the separation by mutual coalescence. In the case of the slow start of the solidification after the separation, they formed a clear interface between the upper cobalt-enriched layer and the lower copper-enriched layer located in the lower part according to the density difference between the two melts. It depended on the cooling rate after liquid separation. The very fine duplex structure can be obtained by the rapid cooling of the melt at the initial stage of the separation.

1. Introduction

The equilibrium phase diagram (Fig. 1) of the Co–Cu alloy system [1] shows a flat liquidus line similar to that of the Fe–Cu system. From the thermodynamics data [2], this system has a large positive deviation of activity of the components in liquid solution from Raoultian behaviour. It is known that this system has a metastable liquid miscibility below the liquidus [3–5], as does the Cu–Fe system [3, 6–8]. This alloy will be expected to show the liquid separation depending on the degree of undercooling.

Nakagawa *et al.* [3] first reported the separation in the Co–Cu system after measuring the magnetic change during the undercooling. The minimum undercooling for the liquid separation was defined as the temperature difference between the equilibrium liquidus and the metastable liquid miscibility temperature gap. That value [2] in the Co–Cu system was much higher than that in the Fe–Cu system. Therefore, it was rather difficult to achieve the liquid separation in the Co–Cu system owing to the higher minimum undercooling. Munitz *et al.* [4, 5] also reported the separation achieved by using a drop tube technique, an electromagnetic levitation, or electron-beam surface melting. However, there are still few detailed reports on the undercooling behaviour in this system. In this study, we examined the undercooling behaviour by thermal analysis during the solidification and its effect on the solidification structure.

2. Experimental procedure

Various $Co_{100}Cu_{100-x}$ ($x = 20, 30, 50, 70$) alloys were prepared from 99.9% purity electrolytic cobalt and copper. In some $Co_{40}Cu_{60}$-based alloys, a small amount of B(0.1, 0.3 and 1.0 at %) was added. The reason for the addition of boron was based on our preliminary experiment, where boron was found to be a quite effective element for the liquid separation, in addition to carbon, in the Fe–Cu system [3].

About 50 g of alloy was melted in an alumina crucible using a high-frequency induction furnace under an argon gas atmosphere, as shown in Fig. 2. When the melt reached a given temperature, the power to the high-frequency induction furnace was turned off. Then the specimen was slowly cooled to 1300 K in the furnace. After complete solidification, the specimen was heated again to the given temperature. These procedures were repeated several times. In this paper, the first set of heating and cooling cycles is denoted

[‡] Formerly graduate student of Osaka University. *Present Address*: Cold Rolling Plant, Kimitsu Works, Nippon Steel Corporation Kimitsu, Chiba 299-11, Japan.
[§] Visiting Scientist at Osaka University. *Present Address*: Department of Control Engineering, Nara National College of Technology, Yata-machi 22, Yamato-Koriyama-shi, Nara 639-11, Japan.

0022–2461

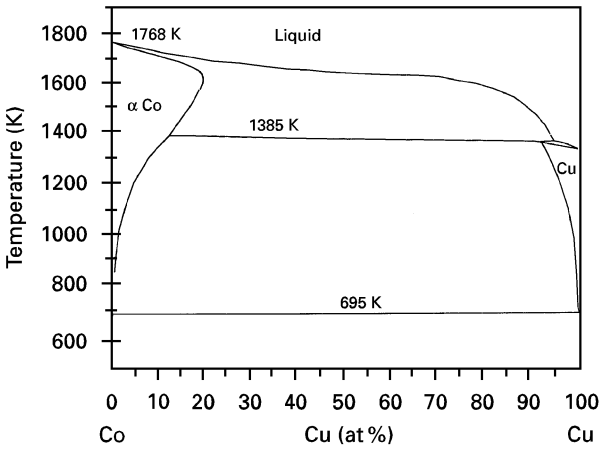

Figure 1 Equilibrium phase diagram of the Cu–Co system [1].

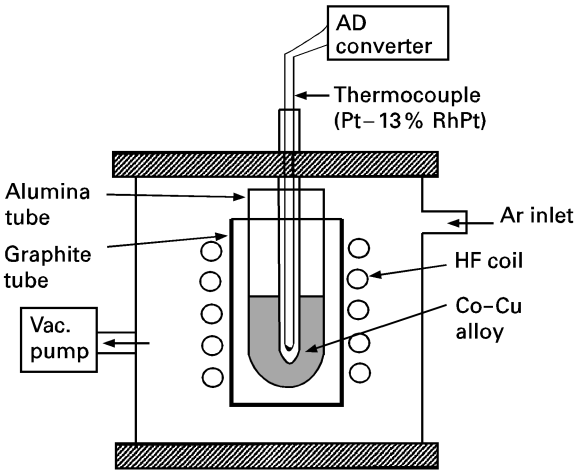

Figure 2 Schematic illustration of equipment used for the static undercooling experiment.

Run 1, and so on. The temperature change during each Run (cycle) was measured using a Pt–13%RhPt thermocouple placed in the central part of the specimen in the crucible and it was recorded using a microprocessor through an AD converter. The recorded data were analysed under Newtonian cooling assumption, as described later.

In some experiments, the specimen in the *n*th cooling stage was cooled to room temperature in the furnace without the next re-heating stage. Thus, some specimens having just temperature data were obtained to examine the effect of the undercooling on the microstructure.

The microstructure of these specimens was observed using the back-scattering image (BEI) of SEM after light etching by a dilute HNO_3 solution for a few seconds.

3. Analysis of temperature data

Because the measured temperature data will reflect the solidification behaviour, they were analysed assuming Newtonian cooling conditions, i.e. the temperature distribution in the specimen is negligibly small. First, the propriety of the Newtonian cooling assumption was examined. We assume that the cooling of the specimen is controlled only by the convection through the outer surface of the crucible. The overall heat-transfer coefficient, h, was roughly evaluated to be about $70\,\mathrm{W\,m^{-2}K^{-1}}$ from the measured cooling curve. The average thermal conductivity, λ, of the specimen was about $176\,\mathrm{W\,m^{-1}K^{-1}}$ and the representative dimension d (here, the diameter of the crucible) was $2.4\times10^{-2}\,\mathrm{m}$. Thus the Biot number ($= hd/\lambda$) is about 0.01. The assumption of Newtonian cooling conditions will be established for such a low Biot number [9]. Therefore, in this experiment, the temperature distribution in the specimen is so small that the measured temperature will represent the temperature of the whole sample.

The temperature during cooling of the superheated melt initially decreases monotonically under plain cooling conditions, which indicates cooling without any endothermic or exothermic reaction because of no phase transformation. When the solidification or any other transformation starts, the temperature will deviate from the plain cooling conditions by the heat generation due to the latent heat. The amount of the heat generation can be calculated from the deviation of the cooling curve from the plain cooling.

By Newtonian cooling conditions, the heat balance equation is described by

$$C_p\rho V(\mathrm{d}T/\mathrm{d}t) = -hS(T-T_a) - \varepsilon\sigma S[(T+273)^4 - (T_a+273)^4] + V\rho(\mathrm{d}q/\mathrm{d}t) \quad (1a)$$

where C_p is the specific heat, ρ the density, ε the emissivity, h the overall heat transfer coefficient between alloy and ambient atmosphere, σ the Stefan–Boltzman constant, t the time, q the internal heat generation rate per unit mass, T the temperature, T_a the ambient temperature, S the surface area of the specimen, and V the volume of the specimen. The term on the left of Equation 1a represents the accumulated thermal energy in the specimen per unit time. The first term on the right is the thermal energy lost by the convective heat transfer. The second term on the right is the heat lost by radiation. Finally, the third term is the thermal energy generation by phase transformation. If the second term is neglected, Equation 1a can be rewritten as

$$C_p\rho V(\mathrm{d}T/\mathrm{d}t) = -hS(T-T_a) + V\rho(\mathrm{d}q/\mathrm{d}t) \quad (1b)$$

When the sample is in the course of the phase transformation, the heat generation term should be taken into account. However, this term can be omitted in the plain cooling condition as described by

$$C_p\rho V(\mathrm{d}T/\mathrm{d}t) = -hS(T-T_a) \quad (1c)$$

Equation 1c can be integrated from $T = T_{max}$ at $t = 0$ to $T = T$ at $t = t$

$$\ln[(T-T_a)/(T_{max}-T_a)] = -[hS/(C_p\rho V)]\,t \quad (2)$$

By differentiating Equation 2 by t,

$$\mathrm{d}\ln\{(T-T_a)/(T_{max}-T_a)\}/\mathrm{d}t = -hS/(C_p\rho V) \quad (3)$$

The right-hand side of Equation 3 is replaced by θ, to give

$$\theta = -hS/(C_p \rho V) \quad (4)$$

θ is also approximately described by the small change of temperature for small time increment, Δt, by Equation 5 from Equation 3

$$\theta = \Delta[\ln(T - T_a)/(T_{max} - T_a)]/\Delta t \quad (5)$$

where $\Delta[\ln(T - T_a)/(T_{max} - T_a)]$ means the variation of $[\ln(T - T_a)/(T_{max} - T_a)]$ during a small time interval, Δt.

When the solidification starts, the internal heat generation due to it should be evaluated.

By rearranging Equation 1b and substituting θ as described in Equation 4

$$dq/dt = C_p[dT/dt - \theta(T - T_a)] \quad (6)$$

The value θ can be experimentally obtained from the plain cooling curve by using Equation 5. The dT/dt (cooling rate) and T on the right-hand side of Equation 6, and T, can be also obtained from the temperature–time curve. Because all of the values on the right-hand side of Equation 6 are given, the internal heat generation rate, dq/dt on the right-hand side of Equation 6 can be calculated. The sum of each dq from the start to the end time of the solidification is equivalent to the latent heat of the solidification, H. The solid fraction variation rate, df_s/dt, is given by

$$df_s/dt = (dq/dt)/H \quad (7)$$

By numerical integration of Equation 7, the fraction of solid, f_s, during the solidification can be evaluated.

4. Results and discussion

4.1. Effects of cyclic heating and cooling on the undercooling

Fig. 3 shows an example of the temperature–time and heating rate curve during the first heating stage (Run 1) in an experiment using a $Co_{50}Cu_{50}$ alloy. There were two minima in the heating rate curve which was obtained by numerically differentiating the temperature–time curve. The first and second minima were revealed at 1360 and 1645 K, respectively. The former corresponded to the peritectic temperature, although it was slightly lower than 1385 K (the equilibrium temperature), and the latter was the equilibrium liquidus temperature of the $Co_{50}Cu_{50}$ alloy [1].

Fig. 4 shows several heating curves obtained in different heating cycles (RUNs) of the same sample. All of the curves show almost the same temperature–time patterns. This clearly indicates that the peritectic and liquidus temperatures were the same.

Fig. 5 is an example of Run 7 during the cooling stage of the same sample as in Figs 3 and 4. Several inflection points were observed in the cooling stage. The first inflection, shown as A in Fig. 5, was observed at about 25 s and its temperature was about 1549 K; it was much below 1645 K which was the equilibrium

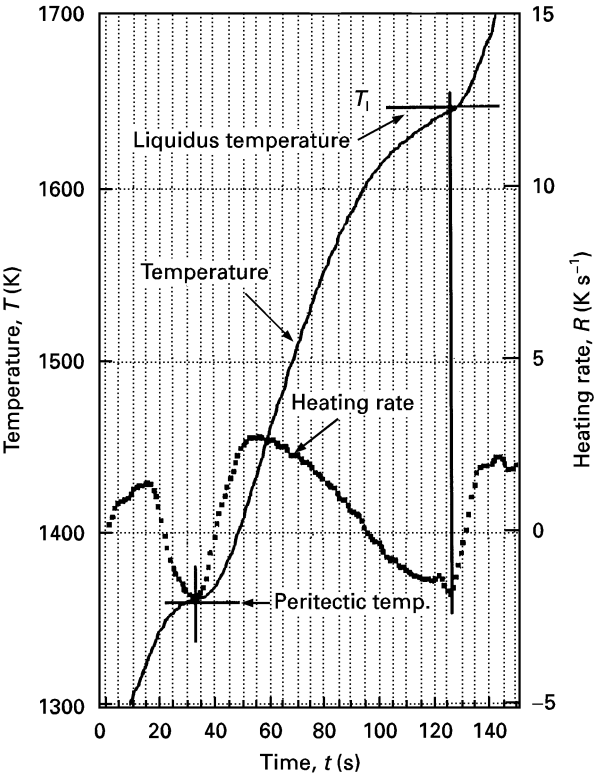

Figure 3 Temperature and heating rate variations with time during the first heating (Run 1) in a $Co_{50}Cu_{50}$ alloy.

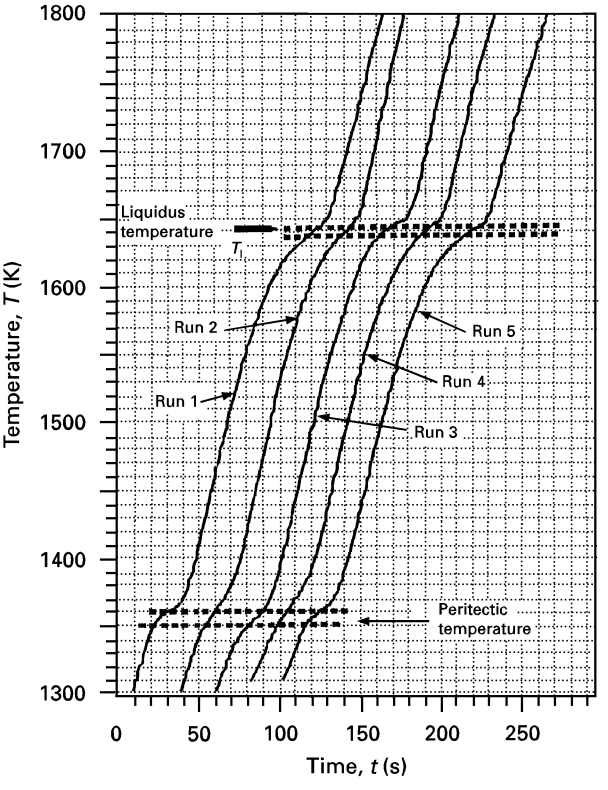

Figure 4 Temperature and heating rate variations in several heating Runs in $Co_{50}Cu_{59}$ alloy.

liquidus temperature obtained by the heating experiment shown in Fig. 3. The temperature change at A was rather small. This temperature, T_s, at A was the start of the liquid separation in the undercooled melt. The undercooling of the melt then continued, accompanied by the liquid separation. The temperature

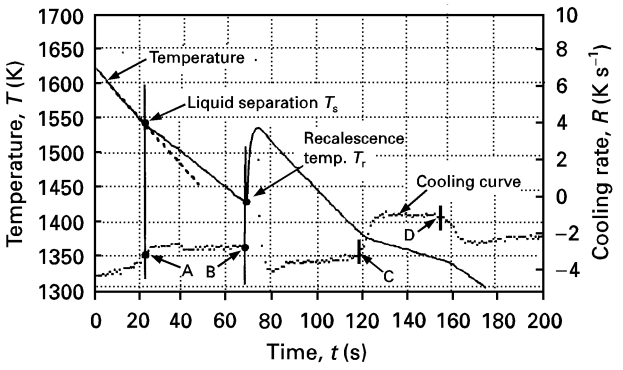

Figure 5 An example of temperature and cooling rate variations in Run 7 of the $Co_{50}Cu_{50}$ alloy.

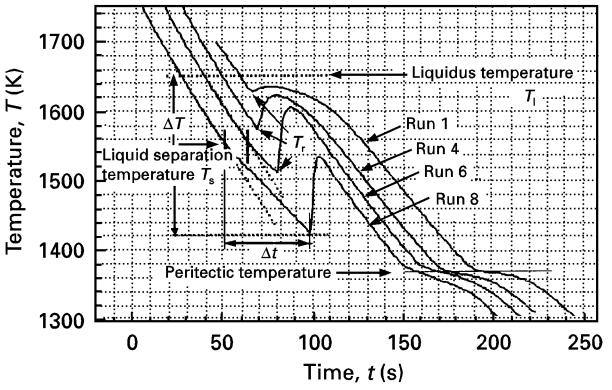

Figure 6 Temperature variations in several cooling Runs in $Co_{50}Cu_{50}$ alloy.

suddenly rose at about 1425 K (B in Fig. 5) due to the generation of latent heat by the solidification. The temperature at point B (recalescence point) was defined as the solidification start temperature, T_r. The third inflection (shown as region C in Fig. 5) started at around 1350 K corresponding to the start of the peritectic solidification. Finally, the fourth inflection (shown as region D in Fig. 5) was at the end of the peritectic solidification. There was a slight temperature difference between regions C and D. When the liquid separation occurred, the melt separated into two liquid layers in the crucible according to the density difference. In the ordinal peritectic reaction, some undercooling was usually observed from the complexity of the solidification behaviour [10]. Therefore, the peritectic reaction in each melt will occur at a slightly different temperature and the resultant peritectic temperature will extend.

Fig. 6 shows the temperature–time curves in the different Runs during the cooling stage. They varied remarkably with the number of Runs. The undercooling increases with increasing number of Runs. The inflection A was first observed after Run 5 and its temperature, T_s, for Run 5, Run 6, Run 7 and Run 8 was about 1549 K, and it was not affected by the number. In Run 1 and Run 4, T_s was not detected, but only T_r was observed. The temperature, T_r in Run 4 was lower than that in Run 1, but it was still higher than T_s. This suggests that the solidification started without the liquid separation. On the other hand, in Run 6, T_r became slightly lower than T_s. So in this case, it is expected that liquid separation probably occurred. We will discuss the undercooling on the solidification structure in detail later.

The liquidus and the liquid separation temperatures in different alloys were similarly obtained and they are summarized in Table I. Thus experimentally obtained miscibility gap temperatures, T_s, were rather lower than those calculated by Hasebe [2]. Table I clearly shows that the addition of a small amount of boron was quite effective to decrease the equilibrium liquidus temperature and to increase the liquid separation temperature. The temperature gap between the liquidus and the liquid separation temperature became smaller on the addition of boron. In other words, the degree of minimum undercooling for the liquid separation decreased on the addition of boron. As a result,

TABLE I Summary of liquidus temperature, T_l, and liquid separation temperature, T_s, by static undercooling experiments

Composition (at %)	Liquidus temperature (K)	Liquidus separation temp. (K)
20Co80Cu	1605	1518
50Co50Cu	1654	1549
70Co30Cu	1680	1499
40Co60Cu	1649	1558
40Co60Cu0.01B	1647	1557
40Co60Cu0.03B	1638	1552
40Co60Cu0.01B	1628	1561
40Co60Cu1.0B	1605	1601

boron may be an effective element to facilitate liquid separation.

The mean cooling rates after liquid separation also seem to be same for the different Runs, as shown in Fig. 6. Therefore, the time interval (Δt in Fig. 6) which was defined as the period between the start of the liquid separation and the start of the solidification, increased with increase of the Run number. When the Δt is sufficiently long to form two melt layers, according to the density difference, each melt will solidify independently, and in the other case, two melts may solidify with some interaction, though this has not been clearly examined.

Variations of θ in $Co_{50}Cu_{50}$ alloy were derived as a function of time from Equation 5 and they are shown in Fig. 7. From Equation 4, θ in the plain cooling period depends on only the apparent heat-transfer coefficient, h, if the thermo-physical properties are constant. The intrinsic heat-transfer coefficient is seen to be almost constant. However, the aparent heat transfer, which includes the radiation, will vary with temperature. It is reasonable for θ, described by the dashed line in Fig. 7, to show a small variation with time (temperature). Also, almost the same values of θ suggest a similar heat-transfer condition in each run. The deviation of θ from the dashed line was caused by the heat generated by the transformation, such as liquid separation or solidification. Fig. 7c and d show that the first small deviation from the dashed line arose from the liquid separation.

The df_s/dt was evaluated from Equations 5 and 6 using the deviation of θ. The f_s was also obtained

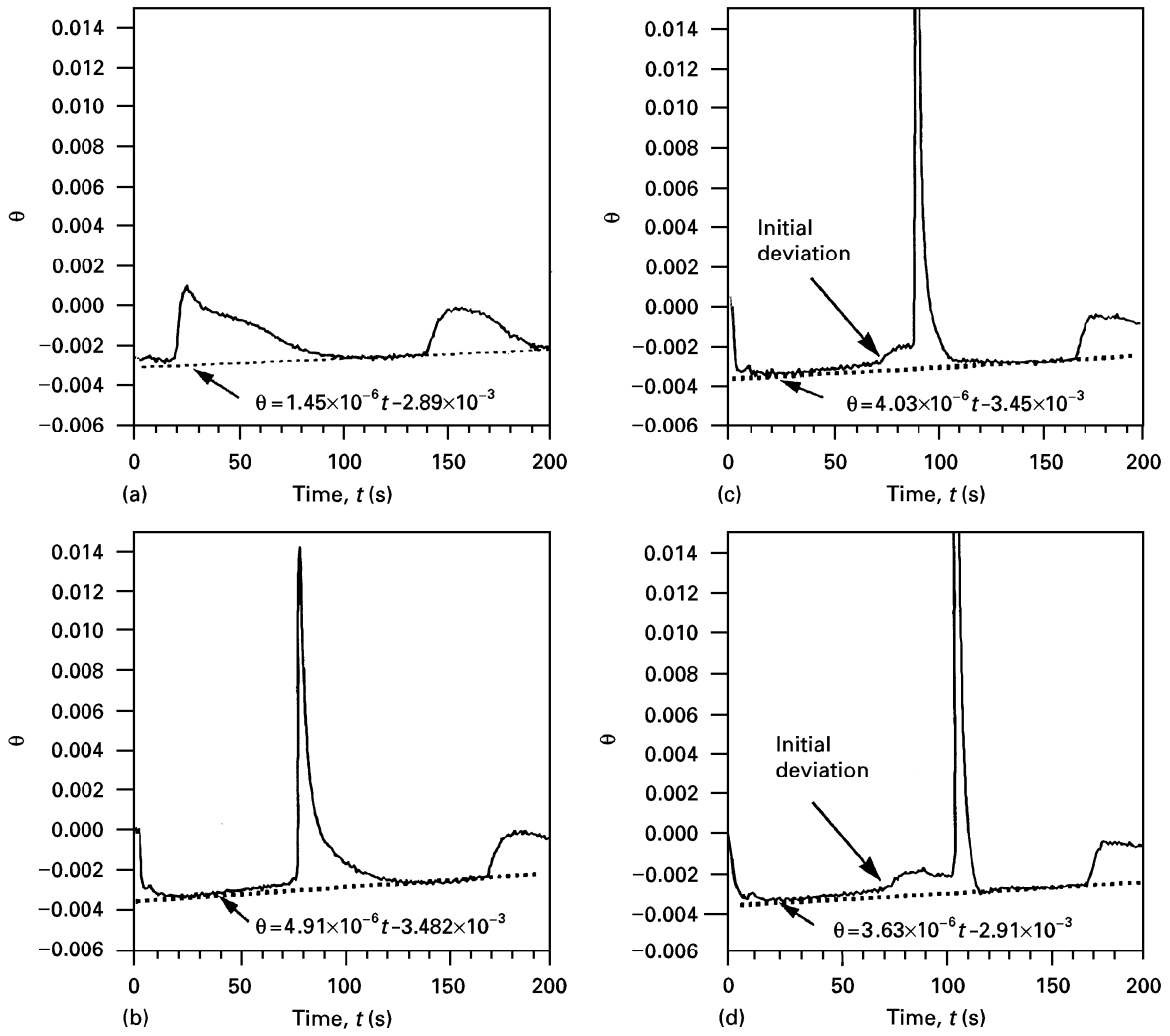

Figure 7 Variation of θ with time and the number of Runs in $Co_{50}Cu_{50}$ alloy. (a) Run 1, (b) Run 4, (c) Run 6, (d) Run 7.

by integrating Equation 6. These results are shown in Fig. 8. In this analysis, the exothermic heat caused by liquid separation was excluded. In Run 1, the solidification rate df_s/dt first increased then gradually decreased to zero and finally increased again according to the start of the peritectic reaction. The solidification started with a different degree of undercooling in each Run. The solidification rate also depended on the undercooling. In Run 4, the undercooling was much higher than that of the Run 1. Therefore, it is reasonable that the solidification rate in Run 4 was much higher than that in Run 1. On the other hand, in Run 6 and Run 7 where the liquid separation occurred before the solidification, the solidification behaviour was quite similar in both Fig. 8c and d. The solidification rate was quite high at the beginning of the solidification and about 60% of the melt solidified within a few seconds after the solidification started. Run 6 and Run 7 had significantly different values of Δt. A different solidification behaviour will be expected from the different degree of separation. However, it was difficult to find any significant difference between them. One of the reasons why the difference could not be clearly detected, is that the sampling interval of 1 s in the temperature measurement, is too long to detect the difference. However, the reason is not still proved and this will remain a topic in further work.

The f_s versus time curve shows almost a plateau at the fraction between 0.6 and 0.7 in the different Runs. The temperature at the plateau corresponds to the peritectic temperature of Co–Cu, as shown in Fig. 6. After the peritectoid started, the solidification progressed similarly in all Runs except for the slight broadening of the peritectoid reaction temperature range at the higher numbers of Runs.

4.2. Effects of undercooling on solidification structure

Fig. 9 shows an example of the microstructure of the statically undercooled specimen with different undercooling in $Co_{50}Cu_{50}$ alloys. For the smaller undercooling ($\Delta T = 65$ K) ($T_r > T_s$), only a typical dendritic structure was observed and there was no evidence of liquid separation (Fig. 9a). In this case, the primary dark dendritic phase was a cobalt-enriched phase, and the interdendritic white phase was copper-enriched phase. However, no typical peritectoid structure was observed. For the larger undercooling ($\Delta T = 123$ K) ($T_r < T_s$), the solidified structure was quite different from the above-mentioned structure.

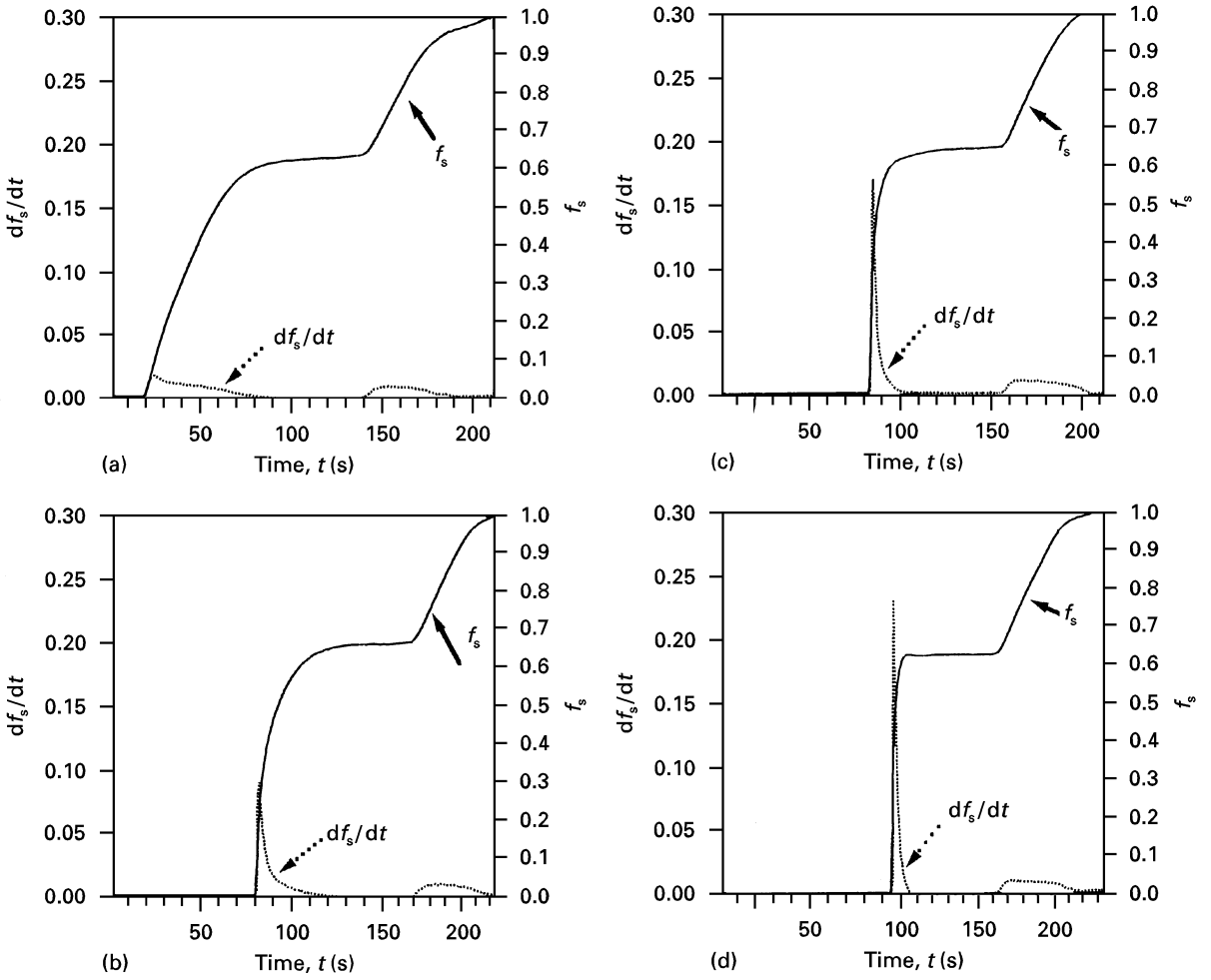

Figure 8 Variation of solid fraction and solidification rate with time and the number of Runs. (a) Run 1, (b) Run 4, (c) Run 6, (d) Run 7.

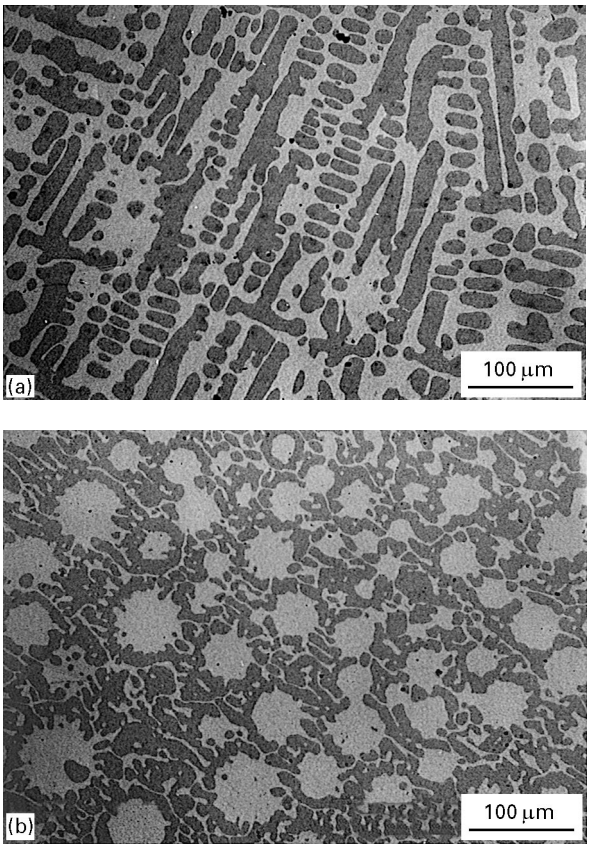

Figure 9 The effect of the degree of undercooling (ΔT), on the microstructure of the $Co_{50}Cu_{50}$ sample. (a) $\Delta T = 65$ K, (b) $\Delta T = 123$ K.

Fine white spherical structures (copper-enriched phase) in various sizes were observed in the dark cobalt-enriched matrix, and the spherical structure extended with some protrusions to the peripheral dendritic region (Fig. 9b). In this case, the time interval, Δt, which was defined in Fig. 6, was 18 s and it was so short that the chance of coalescence of each liquid droplet was relatively low. Thus the spherical structure was observed. Also, dark dendritic structures were observed in the inter-droplets region. These results suggest that two melts with different composition were solidified by rejecting the solute, and some interaction occurred at the interface of the two melts.

To allow further discussion of the observed structure, it is better to suppress the high-temperature state by quenching the specimen from various temperatures.

For the highest undercooled specimen ($\Delta T =$ 196 K), liquid separation also occurred. In this case, the time interval, Δt, was 50 s and it was too long for each drop to become larger by coalescence of the drops. The two kinds of coarser liquid drops moved quickly and vertically, according to Stoke's law, due to their density difference. Finally, two completely separated melt layers were formed for a sufficiently long Δt.

Fig. 10a shows the structure in the vicinity of the two-melt layer interface of the above sample. The white lower part (L_2) is a copper-enriched region and the upper dark part (L_1) is a cobalt-enriched region.

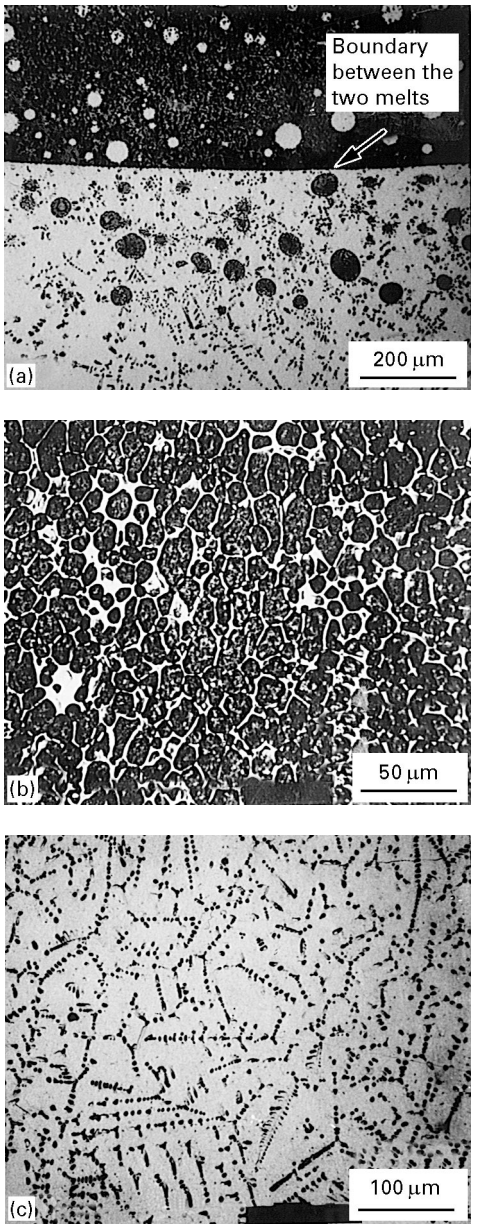

Figure 10 Microstructure of a liquid-separated specimen in the $Co_{50}Cu_{50}$ alloy ($\Delta T = 196$ K): (a) the boundary between the two melts, (b) cobalt-rich region (upper part), (c) copper-rich region (lower part).

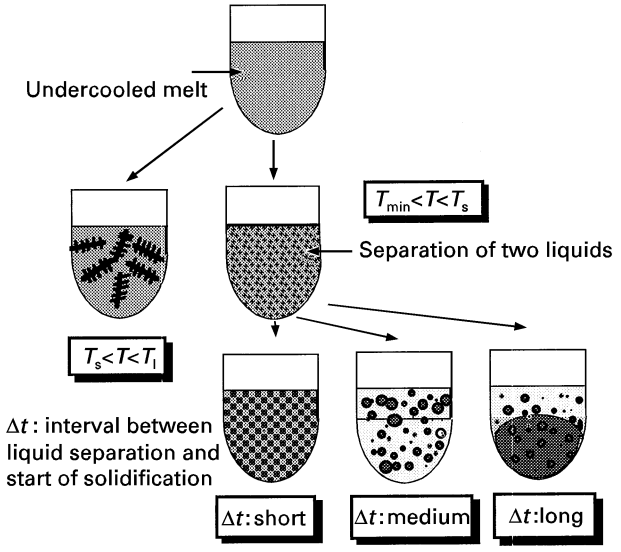

Figure 11 Schematic illustration of the sequence of solidification at various cooling rates.

Some droplets in the different melt (L_1 and L_2) layers were still observed in the neighbourhood of the interface. Thus liquid separation continued in this region. Slightly further away from the interface, the solidified structure was quite different from that at the interface. It was typically dendritic and not spherical. All of the structures were formed by the independent solidification of each melt without further liquid separation.

The microstructure formation process after the liquid separation is schematically shown in Fig. 11. The top of the figure shows only the undercooled melt before solidification. When the solidification starts in the temperature range of T_r and T_s the dendritic structure will be formed similarly to conventional solidification, as shown on the left of the second row of Fig. 11. On the other hand, when the melt temperature decreases below T_s, then separation of the two melts

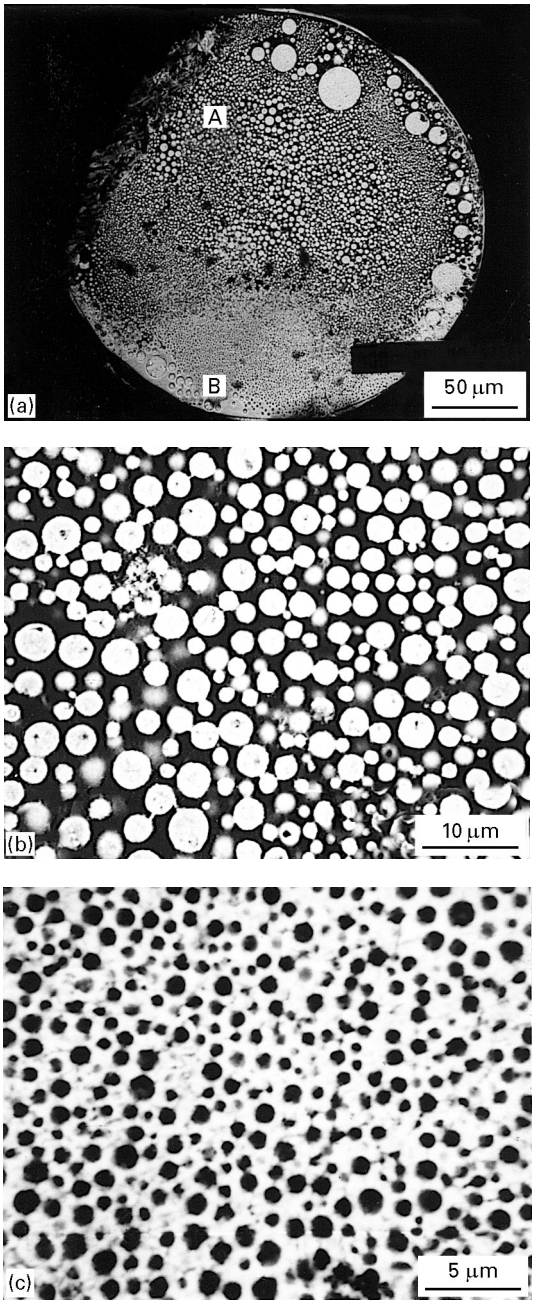

Figure 12 Microstructure of rapidly solidified powder of $Co_{49.75}Cu_{49.75}B_{0.5}$ alloy. (a) Cross section of powder, (b) enlargement of A in (a), (c) enlargement of B in (a).

starts, as shown on the right of the second row of Fig. 11. Very fine liquid droplets will be formed at the beginning of the liquid separation by a similar mechanism of spinodal decomposition. These droplets are usually not very stable, and sometimes they coalesce each other and become larger. If the time interval, Δt, is too short for coalescence to occur, a very fine dispersed duplex structure will be formed, as shown on the left of the third row of Fig. 11. If Δt is much longer allowing coalescence, the two melts move in a vertical direction, according to the in density difference. Then they will independently solidify, as shown on the right of the third row of Fig. 11. Therefore, Δt is an important factor to specify the solidification morphology of the undercooled melt.

If rapid solidification processes apply to this alloy system, a large dynamical undercooling will be easily attained, so that liquid separation will easily occur and the time interval, Δt, will be very short. Therefore, we can expect the finely dispersed duplex structure. Fig. 12 is an example of the rapidly solidified structure of a water-atomized particle [11], although the structure was not homogeneous. In Fig. 12a, the upper part of the particle, a few coarse white droplets were observed in a dark matrix. In the middle part of the particle, very fine dark droplets were observed in a white matrix, as shown in Fig. 12b. On the other hand, in the lower part of the particle (Fig. 12c), the contrast of the droplets was reversed with that of the Fig. 12b.

These results suggest that the finely dispersed duplex structure can be produced by the rapid quenching of the alloy with a metastable liquid miscibility gap [1].

5. Conclusions

1. The degree of undercooling in the Co–Cu alloys increased with the number of heating and cooling cycles.

2. The addition of small amounts of boron was effective in increasing the undercooling.

3. Separation of two melts was clearly detected by the temperature measurement and the analysis based on the Newtonian cooling assumption. It occurred when the liquid was undercooled below the metastable liquid miscibility gap temperature.

4. The metastable miscibility gap temperature only depended on the alloy composition in B free alloys.

5. After the liquid separation, the two melts became coarser by the coalescence of each drop and the final solidified structure depended on the cooling rate after the liquid separation.

References

1. T. B. MASSALSKY (ed.), "Binary Alloy Phase Diagram", ASM (1986) 760.
2. M. HASEBE and T. NISHIZAWA, *Calphad* **4** (1980) 83.
3. Y. NAKAGAWA, *Acta Metall.* **6** (1958) 704.
4. A. MUNITZ and R. ABBASCHIAN, *J. Mater. Sci.* **26** (1991) 6458.
5. A. MUNITZ, S. P. ELDER and R. ABBASCHIAN, *Metall Trans.* **23A** (1992) 1817.
6. K. IWASE, M. OKAMOTO and T. AMEMIYA, *Sci. Rep. Tohoku Univ.* **14** (1937) 618.
7. P-A. KINDQVIST and B. UHRENIUS, *Calphad* **4**(3) (1980) 193.
8. A. MUNITZ, *Metall. Trans.* **18B** (1987) 565.
9. R. MEHRABIAN, S. C. HSU, C. G. LEVI and S. KOU, in "Rapid Solidification Processing Principles and Technologies", Edited by R. Mehrabian, B. H. Kear and M. Cohen (Claitor's, Baton Rouge, Lousiana, LO, 1980) p. 13.
10. M. HILLERT, "Solidification and Casting of Metals" (The Metals Society, London, 1979) p. 81.
11. I. YAMAUCHI, N. UENO, M. SHIMAOKA and I. OHNAKA, (1995) unpublished work.

Received 23 August 1996
and accepted 22 August 1997